ADVANCED MATERIALS INTERFACES
Open Access
www.advmatinterfaces.de

Structural Spectrum of 2D Materials in Solution: Toward Establishing 2D Assemblies' Digital Factory

Lingfei Wei, Jinguo Lin, Cen Chen, Li Yu, Canhui Lu, and Feng Liu**

The numerous hierarchical architectures of 2D assemblies endow them with a new dimension to realize novel properties. From theoretical perspective, freedoms stem from in-plane and out-plane mechanical properties of 2D materials separately, which makes 2D materials embrace more than one "persistence length" giving rise to the diverse morphologies. However, the understanding of 3D architecture formation in 2D assemblies is still in its infancy. In fact, there is even no theoretical classification or reference to help clarify structural difference among numerous experimental obtained 2D assemblies. Based on the theoretical model composed by 2D sheets and Lennard-Jones liquids, solution concentration dependence of 2D materials conformation is systematically studied, and a ln *K* behavior is uncovered that can realize the theoretical conformation prediction of 2D materials. More importantly, the digital production line (solution processing procedure) is set up toward establishing the 2D assemblies' digital factory. The obtained structures may provide a reference to 2D assemblies, which benefits the understanding of the structural difference among different experiments and even help to guide the experimental design of 2D assemblies with targeted architectures and properties.

1. Introduction

Low-dimensional materials possess remarkable physical properties,[1–4] such as superior mechanical properties,[5–9] excellent thermal and electric transporting properties,[10–15] unique optical functionalities,[16,17] and outstanding electrocatalysis performance.[18–20] An ambitious idea is to integrate low-dimensional materials and tame their properties for applications at macroscale. Along this thought, different strategies have been applied, for instance 0D nanomaterials are served as fillers to reinforce and functionate the polymer,[21,22] while 1D nanomaterial could be also used as fillers or directly assembled,[5,13,23] especially this year nanoscale hypo crystalline ceramic fibers are successfully synthesized to an aerogel that is highly flexible and thermal insulating even at very high temperatures.[24] The processing methods keeps rapidly developing, and the assembling architectures and methods increase monthly. In the period of writing this article, 0D material fullerene (C_{60}) manages to find its way to become an assembly with a suitable band gap as a semiconductor.[25]

However, moving from one dimension to two offers access to surface morphologies, the diversity of which leads to numerous hierarchical architectures for 2D assemblies and endows a new dimension to realize novel properties.[26–31] For example, by just tuning the stacking ways of 2D materials, it is reported on Science that the unique interlayer sliding and rotation degrees of freedom emerge in van der Waals thin films ensuring their extremely high mechanical stretchability, malleability, permeability and breathability.[32] From theoretical perspective, freedoms stem from in-plane and out-plane mechanical properties of 2D sheet separately, which help 2D sheet embrace more than one "persistence length" giving rise to the diverse morphologies.

The feature of multiple characteristic length scales distinguishes 2D assemblies from lower dimension materials' assemblies, and thus attract a surge of theoretical studies. Tethered surface model proposed by Nelson[33,34] is widely accepted and applied to study the conformation of 2D sheet in the dilute limit. At a given temperature a competition between the obtained entropy through out-of-plane wrinkling and enthalpic penalties due to the deformation resistance determines its final conformation.[35] Until now, a lot of different phases has been

L. Wei, C. Lu
State Key Laboratory of Polymer Materials Engineering
Polymer Research Institute at Sichuan University
Chengdu 610065, P. R. China
E-mail: canhuilu@scu.edu.cn

J. Lin, C. Chen, L. Yu, F. Liu
State Key Laboratory of Nonlinear Mechanics
Institute of Mechanics
Chinese Academy of Sciences
Beijing 100190, P. R. China
E-mail: liufeng@imech.ac.cn

J. Lin, C. Chen, L. Yu, F. Liu
School of Engineering Sciences
University of Chinese Academy of Sciences
Beijing 100049, P. R. China

The ORCID identification number(s) for the author(s) of this article can be found under https://doi.org/10.1002/admi.202202310.

DOI: 10.1002/admi.202202310

found such as flat, fold, crumple, flat stacks, multiple folds and multiple crumples, and the corresponding scaling law for a given phase is carefully investigated in the dilute limit.[35–38] Recently, there is a fascinating work which uses machine learning techniques to discover again the different conformations of 2D sheet in dilute solutions and to map their morphology. This data-driven approach extracts key geometric and topological features of 2D sheet.[39] Although this is a good start to establish a theoretical understanding for 2D sheet resembling the chain conformation investigation at the initial stage of polymer physics, a further step needs be taken for a more comprehensive understanding the formation conditions of the various conformation phases and the assembling ways of 2D sheet in the concentrated solution. Its urgence origins from the fact that the thriving 2D assemblies are almost obtained through solution processing, which embraces diverse assembling architectures and consequently versatile applications in energy storage and conversion,[40] electronics,[41,42] biology,[43,44] etc. Comparing to widely studied the conformation of individual 2D sheet, the understanding of 3D architecture formation in 2D assemblies is still in its infancy. In fact, there is even no theoretical classification or reference to help clarify structural difference among numerous experimental obtained 2D assemblies. It is therefore of both fundamental and practical importance for understanding the structure of 2D materials not only in the dilute solution but also concentrated one, which could be taken advantage to predict and even design their assembling styles and physical properties in the end.[45]

In this article, the structural spectrum of 2D materials in solution is systematically studied, focusing on the structural diversity induced by anisotropic mechanical properties and concentration dependence. Especially, a mixing entropy induced ln K behavior is uncovered, which enables the theoretical conformation prediction of 2D materials. More importantly, the digital production line (solution processing procedure) is set up toward establishing the 2D assemblies' digital factory. It offers insights to the formation of 2D assemblies, and identify a theoretical way to predict their structural features, such as porosity and specific surface area.

2. Results and Discussion

2.1. Theoretical Model: 2D Sheet in Lennard-Jones Solution

Here a new theoretical model system is proposed, in which 2D sheet and Lennard-Jones (LJ) solution are included. To the best of our knowledge, it could be the first model to directly consider the interaction between 2D sheet and solution explicitly in addition to the deformation energy of 2D sheet and thermal energy. Phase diagram of LJ substance is shown in **Figure 1**a, with different temperature and density it travels from solid to gas. The

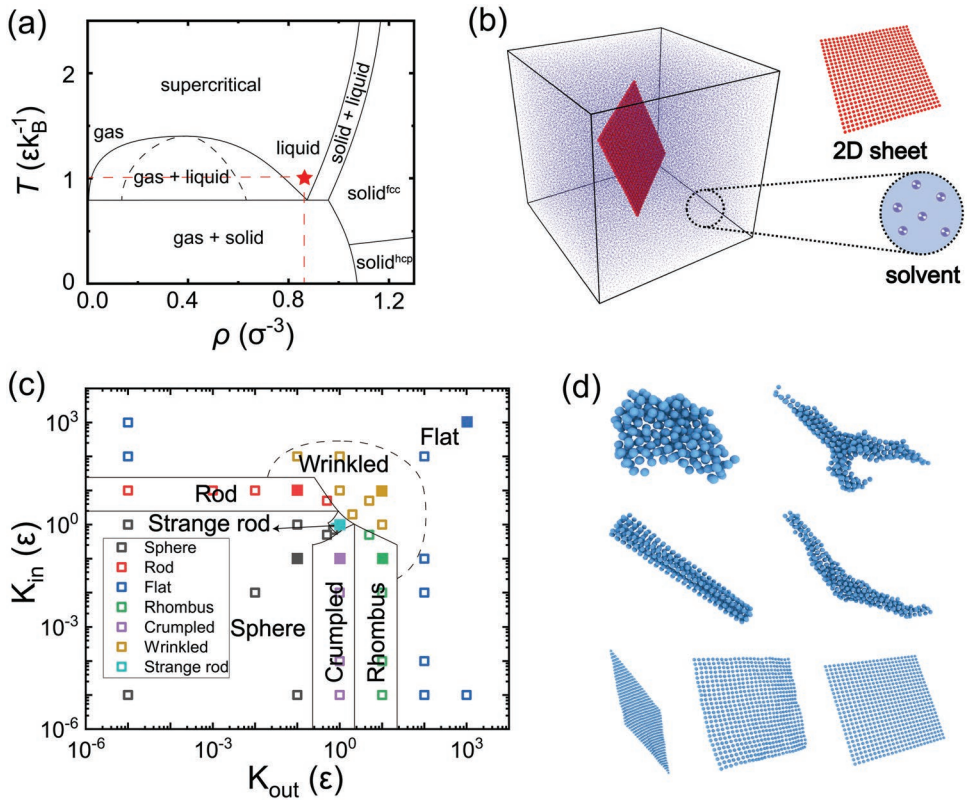

Figure 1. Calculation model and conformation phase diagram. a) Phase diagram of the LJ substance. The red star indicates the selected liquid phase point for all MD simulations ($\rho = 0.87\sigma^{-3}$, $T = \varepsilon$). b) Simulation box contains 108 125 solvent particles and 625 particles belonging to the 2D sheet. c) Phase diagram of the 2D sheet conformation in extreme dilute LJ solution. d) Different conformations presented by 2D sheet in extreme dilute solution. From left to right, and from top to bottom, the conformations are sphere, crumpled branch, rod, strange rod, rhombus, wrinkled, and flat respectively.

chosen state of the LJ substance used in this study is marked with the red star in Figure 1a to guarantee its solution state. Our calculation model is shown in Figure 1b, where a 2D sheet is surrounded by LJ liquid, the possible conformation of 2D sheet is explored. As the conformation of 2D sheet in the dilute limit is determined by the competition between elastic deformation (including both in-plane shear and out-plane bending) and their interaction with LJ liquid. By fixing this interaction and tuning the spring coefficients of the in-plane bond angle K_{in} and that of the out-plane bond angle K_{out}, the conformation of 2D sheet could be comprehensively explored.

The conformational phase diagram of the 2D sheet in the dilute limit is shown in Figure 1c. A total of seven phases are identified here, including all previous founded phases, "flat," "rod," and "crumpled branch."[46] Here the three largest phases are discussed first. When one of the spring coefficients K_{in} and K_{out} is greater than 100ε, the 2D sheet exhibits a "flat" conformation in solution, since the energy of shear or bending deformation of the 2D sheet is so large that the influence of the LJ solution is negligible. As a result, 2D sheet can maintain their initial flat sheet conformation in the solution without wrinkling or folding. However, if the spring coefficients K_{in} and K_{out} are reduced to the order of 10ε, small wrinkles appear on the 2D sheet, which indicates that the shear and bending deformation energy of the 2D sheet approaches the order of the interaction energy between the 2D sheet and the LJ solution. This "winkled" phase is a frequently observed conformation in experiments and widely studied.[35,40,45,47] When the spring coefficients K_{in} and K_{out} are less than 10ε, the shear as well as the bending deformation energy of the 2D sheet can no longer compete with the interaction energy between 2D sheet and LJ solution. In this case, 2D sheet undergoes significant shrinkage and represent a "sphere" or "crumpled branch" conformation in solution, and the dimensionality changes from two to zero.

Plentiful and tiny phases emerge when K_{in} and K_{out} are comparable with the interaction energy between 2D sheet and LJ solution (0.8ε). For example, in the region that K_{out} about 10ε and K_{in} is less than ε, 2D sheet spontaneously transforms into an interesting phase diamond-shaped sheet due to the large bending modulus leading to the unfolding of the 2D sheet while the small shear modulus leading to the conformational change of the 2D sheet in the plane. To be specific, the 2D sheet undergoes in-plane shear deformation, in which the particles rearrange from a square lattice to a more stable rhombus lattice. As a result, the conformation of the 2D sheet changes to "rhombus." In the phase diagram shown in Figure 1c, there are two special conformations, "rod" and "strange rod." When the spring coefficients K_{in} is about 10ε and K_{out} is less than ε, the 2D sheet roll up into a columnar structure along one edge of the sheet during the relaxation process and reduce its dimension to one. It is noteworthy that the formation of the "rod" conformation requires a relative longer relaxation time to reach equilibrium. In our simulation, it takes about 20000τ ($\tau = \sqrt{m\sigma^2/\varepsilon}$), while other conformations take less than 1500τ to reach the equilibrium state. A similar conformation transition is observed when K_{in} and K_{out} are about ε, but its curl is random and uneven, for this reason it is called "strange rod" in this article.

The results of molecular dynamics (MD) simulations show that conformations of 2D sheet in solution are closely related to the shear modulus as well as the bending modulus of the 2D sheet, which are determined by the spring coefficients of the bond angles. Due to generality of our model, which composed by 2D sheet and LJ liquid, the phase diagram could be applied to predict the conformation of 2D materials.

2.2. ln *K* Behavior in the Dilute Limit

Flory–Huggins solution theory[48,49] provides a lattice model to investigate the thermodynamics of polymer solution, and Helmholtz free energy change of mixing per lattice site is given as

$$\begin{aligned}\Delta\overline{F}_{mix} &= \Delta\overline{U}_{mix} - T\,\Delta\overline{S}_{mix} \\ &= K_B\,T\left[\frac{\phi_A}{N_A}\cdot\ln(\phi_A) + \frac{\phi_B}{N_B}\cdot\ln(\phi_B) + \chi\phi_A\phi_B\right]\end{aligned} \tag{1}$$

where $N_A(N_B)$ and $\phi_A(\phi_B)$ are number and volume fraction of substance A (B), and χ is a coefficient quantify the mixing energy. For 2D sheet in LJ solution, A and B correspond to 2D sheet particles and LJ liquid particles respectively. Therefore, $N_A = 1$ and $N_B = 1$, and this equation is rewritten as

$$\begin{aligned}\Delta\overline{F}_{mix} &= \Delta\overline{U}_{mix} - T\,\Delta\overline{S}_{mix} \\ &= K_B\,T\left[\phi_{2D}\cdot\ln(\phi_{2D}) + \phi_{LJ}\cdot\ln(\phi_{LJ}) + \chi\phi_{2D}\phi_{LJ}\right]\end{aligned} \tag{2}$$

where ϕ_{2D} and ϕ_{LJ} represent volume fraction of 2D sheet particles and LJ liquid particles respectively. By taking deformation energy of 2D sheet into account, the total free energy of 2D sheet in LJ solution is given as

$$\overline{F}_{tot} = -K\cdot f\left(R_g(K)\right) + K_BT\left[cK\cdot\ln(cK) + \chi cK + O\left(K^2\right)\right] \tag{3}$$

where the first term is used to describe the increasing deformation energy as the size of the 2D sheet decreases, R_g is radius of gyration and considered as function of K. The second term origins from free energy change of mixing where $\phi_{2D} \approx cK$ and thus $\phi_{LJ} = 1 - \phi_{2D} \approx 1 - cK$ are assumed. Note that with a relatively large modulus 2D sheet unfold and well dissolve in the LJ solution leading to a large mixing entropy, on the contrary with a small modulus 2D sheet curl up into a mass and aggregate without mixing with LJ liquids. At the linear approximation level, it yields $\phi_{2D} \approx cK$. By changing modulus K, plentiful conformational phases emerge (see Figure 1c), and within each phase region the conformation of 2D sheet changes little and the equilibrium condition is given by

$$\frac{d\overline{F}_{tot}}{dK} = -f\left(R_g\right) - K\cdot\frac{df\left(R_g\right)}{dR_g}\frac{dR_g}{dK} + K_BT\left[c\cdot\ln(cK) + c + \chi c\right] = 0 \tag{4}$$

Since in each phase region R_g only weakly depends on K, it brings to an important conclusion that $f(R_g) \sim \ln(K)$. It should be emphasized that this conclusion is applicable for all geometrical characteristics of 2D sheet. This could be seen by substituting $f(R_g)$ with $f(R_g, ..., L_i, ...)$, the above conclusion changes to $f(R_g, ..., L_i, ...) \sim \ln(K)$, where L_i represent ith geometrical characteristic.

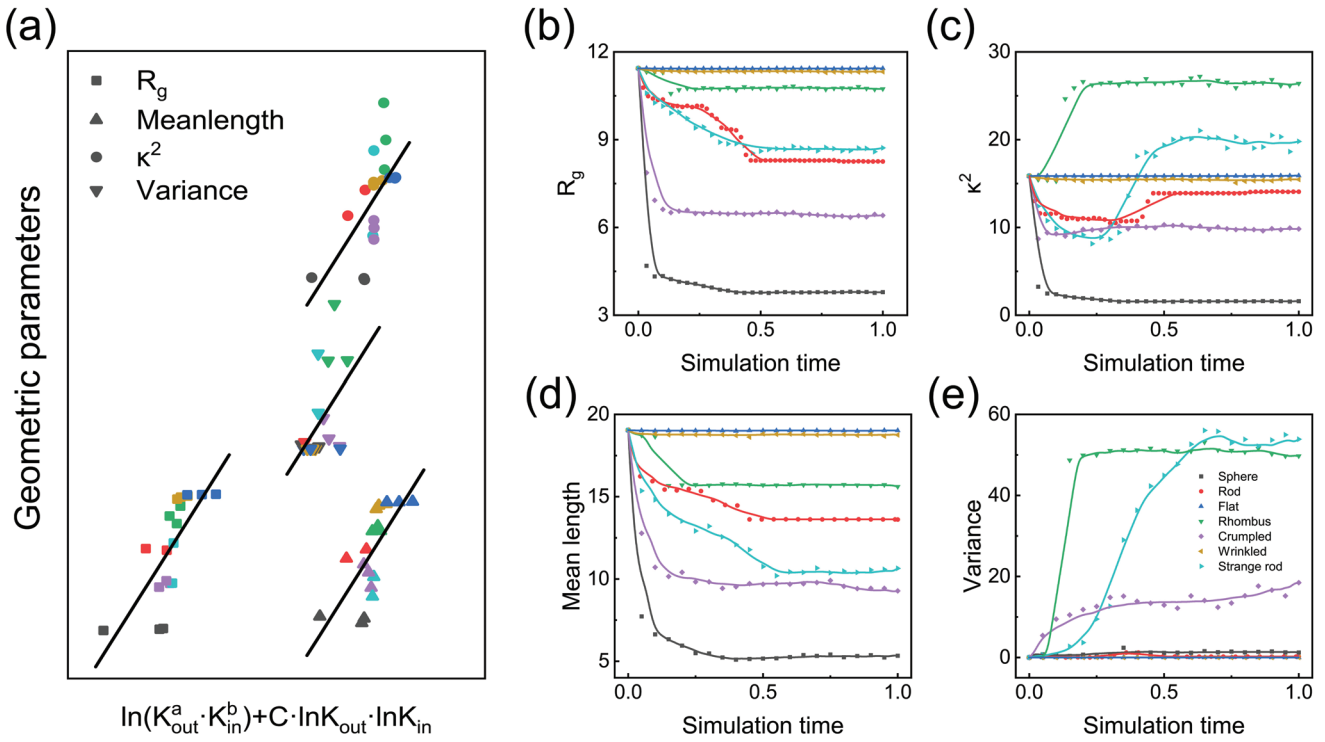

Figure 2. ln *K* behavior of 2D sheet in extreme dilute LJ solution. a) ln *K* behavior of the four geometric parameters. The values of fit coefficients *a*, *b*, and *C* for R_g are 0.4088, 0.1415, and 0.0002, respectively; the fit coefficients for κ^2 are 0.9071, –0.0057, and –0.0270, respectively; the fit coefficients for mean length are 0.7528, 0.1956, and 0.0092, respectively; the fit coefficients for variance are 1.4177, –2.0995, and –0.1726, respectively. Different conformations are marked with different colors, see (e). The evolution of the radius of gyration R_g b), the relative shape anisotropy κ^2 c), mean length d), and variance e) with respect to the simulation time.

To confirm this theoretical relation, four different geometrical characteristics (the definitions could be seen in Supporting Information) are calculated with different K_{in} and K_{out}, and to guarantee statistical significance, about three points for each conformation shown in the phase diagram (in Figure 1c) are taken. As can be seen in **Figure 2**a, all geometrical parameters linear correlates with $\ln(K_{out}^{a} \cdot K_{in}^{b}) + C \cdot \ln K_{out} \cdot \ln K_{in}$, confirming the relation between geometrical characteristics and ln *K*, i.e., $f(R_g, ..., L_i, ...) \sim \ln(K)$. It is worth noting that the presence of the $\ln K_{out} \cdot \ln K_{in}$ term in the linear fit implies that the bending and shear deformation are coupled to a certain degree.

For 1D polymer chains, R_g (the radius of gyration) reflects the degree of "stretching" of the polymer chain. Extending to 2D sheet materials, R_g also describes the degree of "stretching" of the 2D sheet in solution. However, it is clearly not enough to describe the conformation of 2D sheet with only one parameter. For example, the two conformations "rod" and "strange rod" have approximately the same R_g, but are very different in conformation. Therefore, we introduce a second parameter, κ^2 (the relative shape anisotropy), to better describe the conformation of 2D sheet. Their coarse grain versions, i.e., mean length and variance, are also considered and mainly used to confirm *lnK* behavior. The definitions of R_g, κ^2, mean length, and variance could be found in the Supporting Information.

In Figure 2b–e, the evolution of all structural parameters with respect to the simulation time are shown. All structural parameters reached a plateau at the end and stabilized in the later part of the simulation indicating that the 2D sheet have formed different stable conformations after a long enough simulation time. Different types of conformations are discussed separately in the following:

1. The "flat" and "wrinkled" conformations of 2D sheet are essentially the same as the initial conformation, and maintain the 2D character in solution. Therefore, R_g and κ^2 only slightly fluctuate with the simulation time. Similar slight fluctuations are seen for the mean length and variance.
2. The "sphere" and "crumpled branch" conformations of 2D sheet change considerably compared to the initial conformation. The formation of clusters in the 2D sheet results in an overall size reduction, which explains the decrease in R_g and mean length. Due to the greater shrinkage of the "sphere" conformation, both its R_g and mean length are smaller than those of the "crumpled branch" conformation. The shrinking uniformity of the "sphere" and "crumpled branch" conformations is different and leads to the difference in κ^2 and variance.
3. For "rod" and "strange rod" conformations, 2D sheet transforms to 1D rod. These two conformations are similar in shape, and the R_g is also relatively close. However, the two conformations are formed in very different ways. To be specific, the "rod" conformation is coiled, while the "strange rod" conformation is shrunk. The shrinkage makes the κ^2 and variance of the "strange rod" conformation particularly high.
4. The "rhombus" conformation of the 2D sheet still maintains the sheet structure, and the particles are only shifted in the plane of the 2D sheet to form a rhombus-shaped sheet, and

the R_g and mean length decrease due to the dense stacking of particles. The overall shape change resulted in a significant increase in κ^2 and variance.

The radius of gyration, R_g, is considered to be an important parameter to describe the overall dimensions of the 2D sheet, and any folds and shrinkage will reduce R_g to varying degrees. The relative shape anisotropy, κ^2, on the other hand, can effectively identify changes in the overall shape of the 2D sheet, either from 2D to 1D or 2D to 0D transitions. The above analysis shows that the two geometric parameters, R_g and κ^2, can well reflect different conformations of 2D sheet, and thus are used to further identify *lnK* behavior beyond the dilute limit.

2.3. Solution Concentration Dependence of 2D Sheets' Conformation

The different conformations of 2D sheet discussed above are in the environment of extreme dilute solution with large spacing between different 2D sheets. However, in a concentrated solution, the situation is quite different, where the spacing between 2D sheets is so small that they could touch each other.[45] There is an overlapping transition from dilute to concentrated solution, and this transition process has been extensively studied.[50–52] At the onset of the overlapping transition, there exists a critical overlap concentration (C^*), which corresponds to the concentration threshold when a single layer of 2D sheet forms a continuous framework in solution. At this concentration, the solution concentration changes abruptly due to the overlapping between 2D sheet. By measuring the viscosity variation for 2D sheet in LJ solution under different concentration, the overlapping transition concentration could be identified. The viscosity is calculated based on Green–Kubo formalism, the details of which could be found in Simulation Methods.

In dilute solution, i.e., before the overlapping transition, the viscosity of the solution and the concentration are linearly related. As the concentration increases, an abrupt change is expected. Here overlapping transition is carefully studied for all phases. Note that for each phase only one representative configuration is chosen (see solid dots in Figure 1c). As can be seen in **Figure 3**b, the linear relationship between the overlapping transition scale and $\ln(K_{out}^{a} \cdot K_{in}^{b}) + C \cdot \ln K_{out} \cdot \ln K_{in}$ still exists. The viscosity transition processes of the four phases with concentration in MD simulations are shown in Figure 3c–f. The other conformations can be found in the Supporting Information (Figure S1, Supporting Information). The red star in the image mark the points where the viscosity of the solution changes abruptly with concentration. The concentration of the solution corresponding to this point is the overlapping transition concentration. Comparing to the previous structural parameters having only geometrical meaning, overlapping transition length scale has a clear physical significance, and its ln *K* behavior could be much directly measured in experiments to confirm its existence. At the overlapping transition critical point, the system is in a semiconcentrated solution state, this means that the ln *K* behavior may not occur only in the dilute condition.

Since ln *K* behavior is found to be present not only in extreme dilute solution, RDFs (radial distribution function) of solution with different concentrations are further investigated. Figure 3g shows RDFs of all conformations at the overlapping transition point. It could be seen that the highest peak always appears at $r = \sqrt[6]{2}\sigma$, since it corresponds to the equilibrium spacing between particles on the 2D sheet and keeps unchanged for all simulations.

The RDF of the "flat" conformation of the 2D sheet has the sharpest peaks compared to the other conformations. In addition to the peak at the equilibrium distance, there are several distinct sharp peaks on the RDF related to next neighbor equilibrium distance. The particles in the 2D sheet of the "flat" conformation provides a standard RDF and a reference for comparison. The positions of the peaks in the RDF of the "wrinkled" conformation are essentially the same as those of the "flat" conformation, which indicates that these two conformations are very close. Since the small wrinkles of the 2D sheet in the "wrinkled" conformation disrupts the original regularity of the 2D sheet, the smaller and broader peaks of the "wrinkled" conformation are evident in RDFs.

In the "rhombus" conformation, the particles in the 2D sheet are shifted in the same direction, transforming the square 2D sheet into a rhombus shape. The arrangement of the particles is regular, but due to the change in the arrangement, all the peaks except the highest peak at $r = \sqrt[6]{2}\sigma$ are significantly shifted compared to the "flat" conformation.

The "sphere," "crumpled branch," "rod," and "strange rod" conformations of the 2D sheet are different compared to the initial conformation. The "sphere," "crumpled branch," "rod," and "strange rod" conformations of 2D sheet undergo a dramatic shift in their conformations compared to the initial conformations. The dimensionality of the 2D sheet is reduced from two dimensions to one dimension or even zero dimension. The positions of the peaks other than the highest peak in the RDF are different and the peak heights are relatively small, indicating that the particle arrangement of the 2D sheet is irregular.

Figure 3i,j shows the variation of the radial distribution functions of the "sphere" and "flat" conformations at different concentrations. The RDFs of the remaining conformations for different concentrations can be found in the Supporting Information (Figure S2, Supporting Information). Note that the concentration of the extreme dilute solution is $0.005\sigma^{-3}$, while the concentration of the concentrated solution is 1.5 times the transition concentration of each conformation. It can be observed that peaks of the RDF for each conformation barely shift during the increase of the solution concentration, but there is a significant decrease of the peak height. This is because the distance between 2D sheet decreases and they begin to interact with each other, which suppresses the regularity of particles' distribution. The microstructure evolution leads to a smoother RDF (with its peak blunted or even disappearing).

The similar RDFs under different concentration suggest the *lnK* behavior in the dilute limit could be inherited in semiconcentrated or even concentrated solution. In Figure 3k,l, the geometric parameters R_g, κ^2 of the 2D sheet at different concentrations still show a linear correlation with ln *K*. Even though the 2D solution concentration rises and the inter-sheet interaction enhances, the mixing entropy and its induced ln *K* behavior

ADVANCED MATERIALS INTERFACES
Open Access
www.advmatinterfaces.de

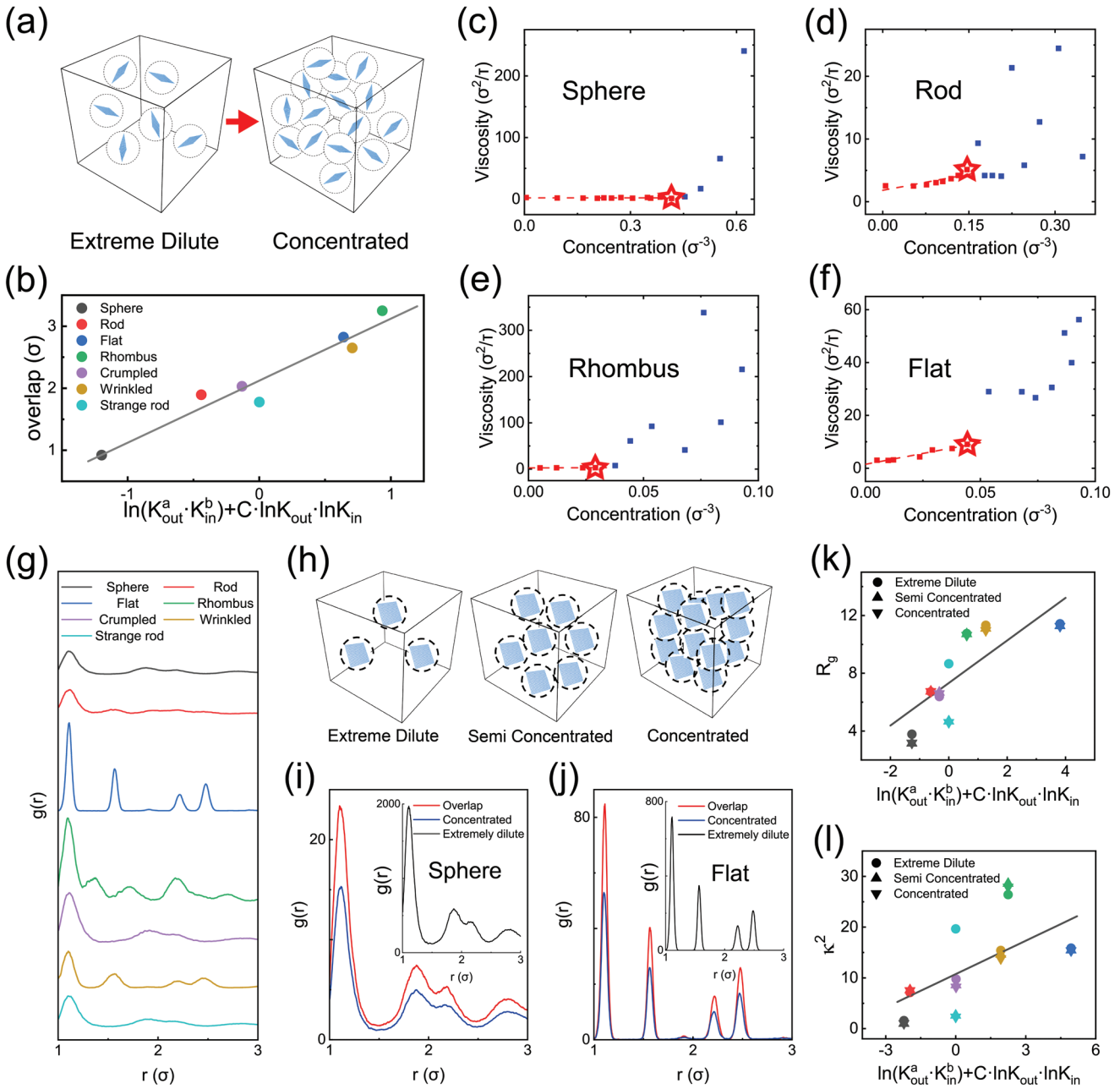

Figure 3. The overlapping transition and solution concentration dependent structure evolution. a) Diagram of the overlapping transition from an extreme dilute solution to a semiconcentrated solution. b) Linear fit of the overlapping transition length scale. The fit coefficients *a*, *b*, and *C* are 0.3562, 0.0574, –0.0465, respectively. Viscosity as a function of concentration for four conformations, which are sphere c), rod d), rhombus e), and flat f). The red star marks the concentration at which the overlapping transition occurs. g) Radial distribution function of 2D sheet particles when the overlapping transition occurs. h) Schematics of the microstructure evolution under different solution concentrations. Radial distribution functions of sphere i) and flat j) conformations at different concentrations. Linear fit of R_g k) and κ^2 l) and the fit coefficients are the same as in Figure 2a, where different conformations are marked with different colors, as shown in (b).

remains unless the concentration is so large at the initial stage that the inter-sheet interaction energy is dominant and solution could barely influence the conformation of 2D sheet.

If the concentration of the 2D solution is less than a critical value, the interaction of the solution with the 2D sheet cannot be neglected and the ln *K* behavior of the solution will always exist. The removal of solvent from the solution during the molding of 2D materials is often uneven. For example, when solvent is removed by drying, evaporation of the solvent takes place in the direction perpendicular to the solution level. Therefore, in addition to isotropic concentrating process, anisotropic concentrating process are also studied. As shown in **Figure 4**b, seven typical conformations are selected (see solid dots in Figure 1c), and five different concentrations

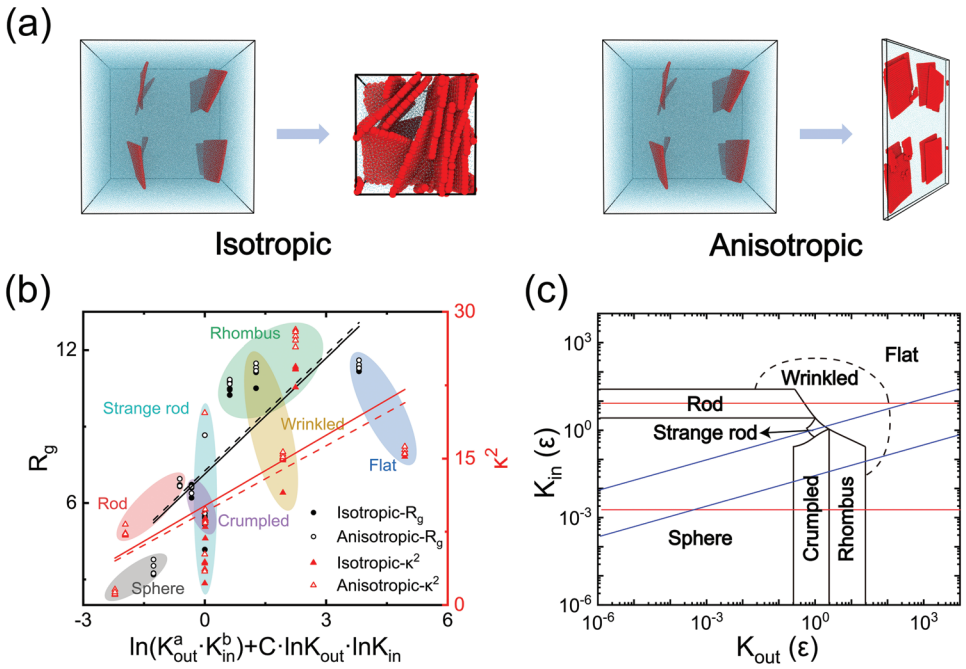

Figure 4. In K behavior during isotropic and anisotropic concentrating processes and the origin of hierarchical architecture for 2D assemblies. a) Microscopic structures under isotropic and anisotropic concentrating. b) In K behavior of R_g and κ^2 during isotropic and anisotropic concentrating processes. The fit coefficients are the same as in Figure 2a. c) The conformation evolution of 2D sheet under the length scale transformation. The blue and red lines represent the changes in side length and thickness of 2D sheet during the assembling process, respectively.

are selected for each conformation. As expected, ln K behavior is present during either isotropic or anisotropic concentrating processes.

The shear modulus and bending modulus of a 2D sheet are closely related to its length scale. In other words, length scale transformation leads to the variation of spring coefficients of in-plane angle K_{in} and out-plane angle K_{out} in calculation model.[53] In Figure 4c, the "flat" and "sphere" phase is used as the initial conformation, the conformational evolution of the 2D sheet under the length scale transformation is shown (by changing either the side length or the thickness of 2D sheet). As both the side length and thickness of 2D sheet could be changed by 2D sheet stacking during the assembling process, the actual conformational evolution should be much more complicated. The behavior found here provides a general route to understand and even predict the conformation of 2D assemblies from nano to micro length scales.

It should be emphasized that the ln K behavior is independent of the calculation model proposed here, it is a consequence of mixing entropy and should exist in all 2D materials' solution, which provides a way to understand and even predict occurrence of conformational phases. In fact, the above-mentioned conformational evolution of the 2D sheet induced by length scale transformation leads to the commonly observed hierarchical architectures in 2D assemblies, since in different length scales 2D sheets tend to assemble themselves using different strategies in the digital production line (see Figure 4c). In term of this recognition, the obtained conformational phase map as well as the ln K behavior provide a principle to design targeted architectures by fine tuning the size of 2D materials and the properties of solution.

2.4. Toward Establishing a 2D Assemblies' Digital Factory

As only the surface can be clearly observed experimentally, the understanding of 3D architecture formation in 2D assemblies is still in its infancy. In fact, there is even no systematical theoretical classification or reference to help clarify structural difference among numerous experimental obtained 2D assemblies. 2D assemblies involving deformation of 2D sheets and strong interactions with liquids remain challenging to model.[54] Based on the proposed theoretical model (composed by 2D sheets and LJ solution), the prototypes of digital production line could be set up in our simulations, in this way 2D assemblies' architecture could be obtained which provides them a structural reference and foundation for classification.

Here, the prototype of digital production line of 2D assemblies is shown in **Figure 5**a. To simulate the experimental processing, temperature is increased from ε to 10ε (heating) and a shear flow field (stirring) is applied. After the solution reaches the equilibrium state system has reached a homogeneous state, the flow field is withdrawn and temperature is gradually reduced to ε (cooling) to form 2D assemblies. Figure 5b shows seven different conformations of the 2D sheet in dilute solution, and the corresponding seven 2D assemblies are shown in Figure 5c, which roughly reproduces all the features observed in the experiments (enlarged view of these structures could be found in Supporting Information).[40–45] Among these assemblies, the "sphere" and "crumpled" belong to 0D conformation, where the 2D sheets are curled into clusters with small hydrodynamic volumes, forming agglomerates in 3D space. The "rhombus ," "wrinkled" and "flat" belong to 2D conformation, and in the corresponding 2D assemblies, they still maintain

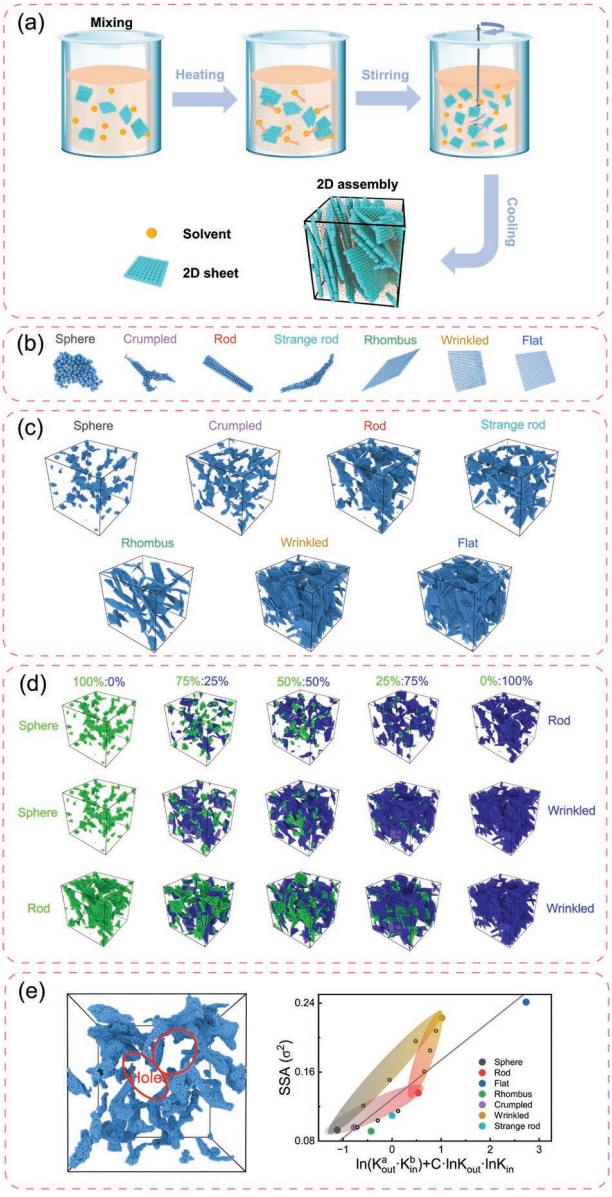

Figure 5. Prototype of digital factory of 2D assemblies. a) Prototype of digital production line of 2D assemblies. b) The different conformations of 2D sheets in dilute solution. c) 2D assemblies with different structures. d) Composite 2D assemblies with different component ratios. e) Schematic diagram of the hole in the 2D assembly and the ln *K* behavior of the specific surface area. The hollow points represent the corresponding composite 2D assemblies. The fit coefficients *a*, *b*, and *C* are 0.1276, 0.3367, and −0.0099, respectively.

the 2D conformation and form a network-like pore structure in 3D space. These pore structures increase the specific surface area of 2D assemblies, giving the possibility of more functional applications of 2D assembly materials. The "rod" and "strange rod" are 1D conformations, and in extreme dilute solutions, the 2D sheets form 1D conformation because they are far apart and do not interfere with each other. However, in concentrated solutions, the 2D sheets are hindered in forming 1D conformation, while some isolate ones can still form a 1D conformation. This class of 2D assemblies can still form 3D network-like pore structures in space, but the specific surface area is smaller because the 2D sheets are more curled up compared to the 2D conformations.

In experiments, two different materials could be combined to endow new physical and chemical properties by means of doping and blending. Their dispersion and structure are widely studied, as they closely related to obtained properties. In the following, the structure of 2D assemblies containing different materials is investigated. Note that only three typical conformations "sphere," "rod," and "wrinkled" are selected as representatives, since their isolated conformations are quite different and exist in the form of 0D, 1D, and 2D, respectively. The structures of the mixed 2D assemblies though pairwise combinations with various proportions are shown Figure 5d (enlarged view of these structures could be found in Supporting Information). The calculated results show that 0D conformation ("sphere") tends to form clusters in the composite system or adhere to the surface of 2D conformation. For 0/1D case (composed by 0D and 1D), if the 0D material is predominant, 2D sheets suffer less intersheet interaction due to the small hydrodynamic volume of the 0D conformation, which gives others better opportunities to form 1D conformation. In terms of these mixed 2D assemblies' structure, it could be found that 1D and 2D conformations play an important role in forming the backbone of the network structure in the composite system.

Besides, the ln *K* behavior in 2D assemblies is studied, which exists for their porosity (Figure S3, Supporting Information) as well as specific surface area (SSA) (Figure 5e) (their definition could be found in Supporting Information). Therefore, in the experiment, we can design the spatial structure of the 2D material by the ln *K* relationship. The simulation results of the two-component 2D assemblies show that the experiments can be done by preparing composite materials, which makes the design of the spatial structure of the 2D materials more tractable and helps to realize the specific functionality of the materials.

Establishing the prototype of digital factory of 2D assemblies helps to provide a structural reference for all 2D assemblies, which benefits the understanding of the structural difference among different experiments, and even help to guide the experimental design of 2D assemblies with targeted architectures and properties.

3. Conclusion

The structural spectrum of 2D materials in solution is systematically studied, in terms of which a ln *K* behavior is identified and prototype of digital factory is established. The former (*lnK* behavior) is a consequence of mixing entropy and should exist in all 2D materials' solutions leading a way to understand and even predict 2D materials' conformational phases and 2D assemblies' architectures. The later (prototype of digital factory) sets a unified structure generation protocol and standard for the follow-up theoretical studies, and could be used to generate 2D assemblies' data bank, which could facilitate the understanding of their formation and even help discover a new processing way in experiments to identify new architectures and functionalities.

4. Simulation Methods

MD Simulations are implemented to explore the conformation of 2D sheet in LJ liquid. The model for 2D sheet is constructed through a square lattice as shown in Figure 1b. The bonds are modeled as linear elastic springs, and the bond angles of 90° and 180° in the square lattice are defined as the in-plane and out-plane angles, respectively. Atoms in the 2D sheet are grouped into beads with equal masses, and the bonding interaction between beads is modeled through a stretching energy term $E = K(r - r_0)^2$, where r_0 is the equilibrium bond distance. The shear modulus as well as the bending modulus of 2D sheet are modeled by harmonic angle potential $E = K(\theta - \theta_0)^2$, where θ_0 is the equilibrium value of the angle, and K is a prefactor. The potential function coefficients for the in-plane and out-plane angles are denoted as K_{in} and K_{out}, respectively. Pairwise interactions between the particles of 2D sheet and solvents are added to the MD field, in the form of Lennard–Jones 12–6 potential $E_{L\text{-}J} = 4\varepsilon[(\sigma/r)^{12} - (\sigma/r)^6]$, with a cutoff distance of 2σ. Here, the equilibrium distance related length σ and energy well ε are 1 for the 2D sheet as a reference. The interaction between the liquid is set to 0.6 and the interaction between sheets and liquids is set to 0.8. The equilibrium distance is 1 for all particles. Lennard–Jones is the prototype for simple and realistic modeling of intermolecular interactions, and thermal properties have been extensively studied and reported in the literature.[55] The computer experimental data of the Lennard–Jones potential are currently considered to be the most accurate data in classical mechanistic computational chemistry. Therefore, a very accurate LJ phase diagram is plotted (Figure 1a).

The MD simulations are performed by using the large-scale atomic/molecular massively parallel simulator (LAMMPS).[56,57] The square 2D sheet has a size of $24\sqrt[6]{2}\ \sigma$ and contains 625 beads. According to the phase diagram of the Lennard–Jones substance (Figure 1a), the density ρ is set to $0.87\sigma^{-3}$ and the temperature T is kept at εk_B^{-1} to ensure that the system is in the liquid state, where the value of k_B in the LJ unit system is 1. Thus, 108 125 solvent particles are added to the simulation box with side length of 50σ. Together with 625 particles in the 2D sheet, there are 108 750 particles in the simulated system and the density is controlled to $0.87\sigma^{-3}$. The energy changes of the 2D sheet as well as the solution system during the relaxation process is monitored to make sure the system reached equilibrium. The deformation energy and assembly energy of the 2D assemblies were also recorded (Figures S8 and S9, Supporting Information).[58] The 2D sheet relaxed in solution for a long enough time to ensure that the system reached an equilibrium state. In order to obtain different concentrations of the solution system, the solvent particles are evaporated while the volume of the simulation box is reduced. During this process, the number density of the system remains constant. After equilibration, the shear viscosity is calculated by the autocorrelation function of the pressure tensor, using the Green-Kubo formalism. By linear fitting of the solution concentration-viscosity image, the points with deviations above 80% of the straight line correspond to the critical overlap concentration. The processing of the 2D assemblies is carried out in a 20% concentration solution. The final obtained 2D assemblies of all types are in solution, and the post-processing process will be performed on the basis of these models.

Supporting Information

Supporting Information is available from the Wiley Online Library or from the author.

Acknowledgements

This study was supported by the National Natural Science Foundation of China (Grant Nos. 11972349 and 11790292), the Strategic Priority Research Program of the Chinese Academy of Sciences (Grant No. XDB22040503), the Sichuan Science and Technology Program (2020YJ0261), the Program for Featured Directions of Engineering Multi-disciplines of Sichuan University (No. 2020SCUNG203), and the Joint Project for the Talent Innovation Sharing Alliance of Quanzhou (2021C064L).

Conflict of Interest

The authors declare no conflict of interest.

Author Contributions

C.L. and F.L. conceived the idea; L.W. performed the molecular dynamics simulations and data analysis. L.W. wrote the initial manuscript. All authors participated in discussing and editing the manuscript.

Data Availability Statement

The data that support the findings of this study are available from the corresponding author upon reasonable request.

Keywords

2D materials, assembly, digital factory, mixing entropy, solution

Received: November 3, 2022
Revised: January 1, 2023
Published online: February 25, 2023

[1] Q. Wu, W.-S. Miao, Y.-D. Zhang, H.-J. Gao, D. Hui, *Nanotechnol. Rev.* **2020**, *9*, 259.
[2] T. Hu, E. Kan, *WIREs Comput. Mol. Sci.* **2019**, *9*, e1409.
[3] H. Xu, H. Shang, C. Wang, Y. Du, *Adv. Funct. Mater.* **2020**, *30*, 2006317.
[4] H. P. Wang, S. Li, X. Liu, Z. Shi, X. Fang, J. H. He, *Adv. Mater.* **2021**, *33*, 2003309.
[5] M. H. Al-Saleh, U. Sundararaj, *Composites, Part A* **2011**, *42*, 2126.
[6] J.-P. Salvetat, S. Bhattacharyya, R. B. Pipes, *J. Nanosci. Nanotechnol.* **2006**, *6*, 1857.
[7] D. Akinwande, C. J. Brennan, J. S. Bunch, P. Egberts, J. R. Felts, H. Gao, R. Huang, J.-S. Kim, T. Li, Y. Li, K. M. Liechti, N. Lu, H. S. Park, E. J. Reed, P. Wang, B. I. Yakobson, T. Zhang, Y.-W. Zhang, Y. Zhou, Y. Zhu, *Extreme Mech. Lett.* **2017**, *13*, 42.
[8] Z. Dai, L. Liu, Z. Zhang, *Adv. Mater.* **2019**, *31*, 1805417.
[9] X. Zhang, W. Lu, G. Zhou, Q. Li, *Adv. Mater.* **2020**, *32*, 1902028.
[10] S. Gong, W. Cheng, *Adv. Electron. Mater.* **2017**, *3*, 1600314.
[11] C. Chen, Y. Fan, J. Gu, L. Wu, S. Passerini, L. Mai, *J. Phys. D: Appl. Phys.* **2018**, *51*, 113002.

[12] H. Sun, J. Deng, L. Qiu, X. Fang, H. Peng, *Energy Environ. Sci.* **2015**, *8*, 1139.
[13] Z. Han, A. Fina, *Prog. Polym. Sci.* **2011**, *36*, 914.
[14] X. Gu, R. Yang, *Annu. Rev. Heat Transfer* **2016**, *19*, 1.
[15] R. Mas-Ballesté, C. Gómez-Navarro, J. Gómez-Herrero, F. Zamora, *Nanoscale* **2011**, *3*, 20.
[16] K. F. Mak, J. Shan, *Nat. Photonics* **2016**, *10*, 216.
[17] K. Thakar, S. Lodha, *Mater. Res. Express* **2020**, *7*, 014002.
[18] M. A. Montiel, F. J. Vidal-Iglesias, V. Montiel, J. Solla-Gullón, *Curr. Opin. Electrochem.* **2017**, *1*, 34.
[19] X. Ren, Q. Lv, L. Liu, B. Liu, Y. Wang, A. Liu, G. Wu, *Sustainable Energy Fuels* **2020**, *4*, 15.
[20] J. Liu, Q. Ma, Z. Huang, G. Liu, H. Zhang, *Adv. Mater.* **2019**, *31*, 1800696.
[21] Prateek, V. K. Thakur, R. K. Gupta, *Chem. Rev.* **2016**, *116*, 4260.
[22] H. Chen, V. V. Ginzburg, J. Yang, Y. Yang, W. Liu, Y. Huang, L. Du, B. Chen, *Prog. Polym. Sci.* **2016**, *59*, 41.
[23] X. Huang, B. Sun, Y. Zhu, S. Li, P. Jiang, *Prog. Mater. Sci.* **2019**, *100*, 187.
[24] J. Guo, S. Fu, Y. Deng, X. Xu, S. Laima, D. Liu, P. Zhang, J. Zhou, H. Zhao, H. Yu, S. Dang, J. Zhang, Y. Zhao, H. Li, X. Duan, *Nature* **2022**, *606*, 909.
[25] L. Hou, X. Cui, B. Guan, S. Wang, R. Li, Y. Liu, D. Zhu, J. Zheng, *Nature* **2022**, *606*, 507.
[26] Y. Wu, N. Yi, L. Huang, T. Zhang, S. Fang, H. Chang, N. Li, J. Oh, J. A. Lee, M. Kozlov, A. C. Chipara, H. Terrones, P. Xiao, G. Long, Y. Huang, F. Zhang, L. Zhang, X. Lepró, C. Haines, M. D. Lima, N. P. Lopez, L. P. Rajukumar, A. L. Elias, S. Feng, S. J. Kim, N. T. Narayanan, P. M. Ajayan, M. Terrones, A. Aliev, P. Chu, et al., *Nat. Commun.* **2015**, *6*, 6141.
[27] L. Qiu, J. Z. Liu, S. L. Y. Chang, Y. Wu, D. Li, *Nat. Commun.* **2012**, *3*, 1241.
[28] Y. Tao, X. Xie, W. Lv, D.-M. Tang, D. Kong, Z. Huang, H. Nishihara, T. Ishii, B. Li, D. Golberg, F. Kang, T. Kyotani, Q.-H. Yang, *Sci. Rep.* **2013**, *3*, 2975.
[29] Q. Shao, J. Tang, Y. Lin, F. Zhang, J. Yuan, H. Zhang, N. Shinya, L.-C. Qin, *J. Mater. Chem. A* **2013**, *1*, 15423.
[30] R. Zhang, Y. Cao, P. Li, X. Zang, P. Sun, K. Wang, M. Zhong, J. Wei, D. Wu, F. Kang, H. Zhu, *Nano Res.* **2014**, *7*, 1477.
[31] H. Ma, H. Chen, M. Wu, F. Chi, F. Liu, J. Bai, H. Cheng, C. Li, L. Qu, *Angew. Chem., Int. Ed.* **2020**, *59*, 14541.
[32] Z. Yan, D. Xu, Z. Lin, P. Wang, B. Cao, H. Ren, F. Song, C. Wan, L. Wang, J. Zhou, X. Zhao, J. Chen, Y. Huang, X. Duan, *Science* **2022**, *375*, 852.
[33] Y. Kantor, M. Kardar, D. R. Nelson, *Phys. Rev. Lett.* **1986**, *57*, 791.
[34] Y. Kantor, M. Kardar, D. R. Nelson, *Phys. Rev. A* **1987**, *35*, 3056.
[35] Y. Wang, S. Wang, P. Li, S. Rajendran, Z. Xu, S. Liu, F. Guo, Y. He, Z. Li, Z. Xu, C. Gao, *Matter* **2020**, *3*, 230.
[36] T. Banerjee, A. Basu, *New J. Phys.* **2018**, *20*, 013028.
[37] Q. Wang, X. Zhao, *MRS Bull.* **2016**, *41*, 115.
[38] L. J. Cote, F. Kim, J. Huang, *J. Am. Chem. Soc.* **2009**, *131*, 1043.
[39] Y. Zhao, J. Qin, S. Wang, Z. Xu, *Patterns* **2022**, *3*, 100497.
[40] Y. Ren, C. Yu, Z. Chen, Y. Xu, *Nano Res.* **2021**, *14*, 2023.
[41] J. Liu, D. Hui, D. Lau, *Nanotechnol. Rev.* **2022**, *11*, 770.
[42] W. Wang, A. D. Schlüter, *Macromol. Rapid Commun.* **2019**, *40*, 1800719.
[43] X. Feng, A. D. Schlüter, *Angew. Chem., Int. Ed.* **2018**, *57*, 13748.
[44] S. Rana, V. Singh, B. Singh, *iScience* **2022**, *25*, 103748.
[45] P. Li, S. Wang, F. Meng, Y. Wang, F. Guo, S. Rajendran, C. Gao, Z. Xu, Z. Xu, *Macromolecules* **2020**, *53*, 10421.
[46] S. T. Knauert, J. F. Douglas, F. W. Starr, *Macromolecules* **2010**, *43*, 3438.
[47] P. Lv, X. Li, Z. Zhang, B. Nie, Y. Wu, N. Deng, H. Tian, T.-L. Ren, G. Wang, *J. Phys. D: Appl. Phys.* **2022**, *55*, 164002.
[48] T. Lindvig, M. L. Michelsen, G. M. Kontogeorgis, *Fluid Phase Equilib.* **2002**, *203*, 247.
[49] A. Sariban, K. Binder, *J. Chem. Phys.* **1987**, *86*, 5859.
[50] Q. Ying, B. Chu, *Macromolecules* **1987**, *20*, 362.
[51] L. Gmachowski, *Polymer* **2006**, *47*, 6257.
[52] X. E. Wilcox, A. Ariola, J. R. Jackson, K. M. Slade, *Biochemistry* **2020**, *59*, 1737.
[53] S. Cranford, M. J. Buehler, *Mater. Sci. Eng., R* **2011**, *19*, 054003.
[54] E. Gao, S. Wang, C. Duan, Z. Xu, *Sci. China Technol. Sci.* **2019**, *62*, 1545.
[55] S. Stephan, M. Thol, J. Vrabec, H. Hasse, *J. Chem. Inf. Model.* **2019**, *59*, 4248.
[56] A. P. Thompson, H. M. Aktulga, R. Berger, D. S. Bolintineanu, W. M. Brown, P. S. Crozier, P. J. in 't Veld, A. Kohlmeyer, S. G. Moore, T. D. Nguyen, R. Shan, M. J. Stevens, J. Tranchida, C. Trott, S. J. Plimpton, *Comput. Phys. Commun.* **2022**, *271*, 108171.
[57] S. Plimpton, *J. Comput. Phys.* **1995**, *117*, 1.
[58] Q. Liu, J. Huang, B. Xu, *J. Mech. Phys. Solids* **2019**, *133*, 103722.